arXiv:1703.08857v1 [math.NA] 26 Mar 2017

Numerical homogenization of time-dependent diffusion

Fredrik Hellman* Axel Målqvist†

March 28, 2017

Abstract

We consider a sequence of elliptic partial differential equations (PDE) with different rapidly varying coefficients. Such equaions appear, for example, in some splitting schemes for time-dependent problems and in sample based stochastic integration of outputs from elliptic equations. This work is based on numerical homogenization by localized computations using the localized orthogonal decomposition (LOD) technique. We propose a parallelizable and memory efficient algorithm that, based on computable error indicators, adaptively recomputes only a subset of the local problems as we iterate the sequence of coefficients.

1 Introduction

In this paper, we consider a sequence of elliptic partial differential equations (PDEs) with different, but in some sense similar, spatially rapidly varying coefficients. One application when such a sequence appears is in simulation of two-phase Darcy flow in a porous medium using a sequential splitting method [5]. That involves solving an elliptic pressure equation with coefficient dependent on the saturation of the two phases. The saturation and thus the diffusion coefficient changes only significantly in a limited region called

*Department of Information Technology, Uppsala University, Box 337, SE-751 05 Uppsala, Sweden. Supported by Centre for Interdisciplinary Mathematics (CIM), Uppsala University.

†Department of Mathematical Sciences, Chalmers University of Technology and University of Gothenburg SE-412 96 Göteborg, Sweden. Supported by the Swedish Research Council.

the front. Another application simulation of random defects in composite materials by a sampling based method, where the coefficient in each sample deviates from a base coefficient only where a defect has occured [1]. In both examples, the difference in coefficient between the problems is localized and there is computational work to save from recomputing the localized problems only where necessary.

The accuracy of Galerkin projection onto standard finite element spaces suffers from variations in the coefficient that are not resolved by the finite element mesh. The work [2] studies an elliptic equation in 1D with rough coefficients and notes that coefficient variations within the element leads to inaccurate solutions for the standard finite element method, but that replacing the coefficient with its elementwise harmonic average leads to an accurate method. This result, however, does not easily generalize to higher dimensions. For periodic and semi-periodic coefficients varying on an asymptotically fine scale, a homogenized coefficient can be computed and used for coarse scale computations also in higher dimensions [4]. The multiscale finite element method [11] is based on this theory under assumptions on scale separation and periodicity. Many recent contributions within the field of numerical homogenization can be used without assumptions on periodicity and in higher dimensions, see e.g. [3, 12, 14, 15, 18]. In this work, we consider the localized orthogonal decomposition (LOD) technique [15] in the Petrov–Galerkin formulation studied in detail in [7].

With the LOD technique, a new low-dimensional function space (multiscale space) with good approximation properties is constructed by computing localized fine-scale correctors to the basis functions of a standard low-dimensional finite element space. The diffusion coefficient appears in the computation of these correctors. Thus, in a situation where the multiscale spaces for several similar coefficients are to be computed, there is an opportunity for reusing previously computed correctors, for example when the coefficient varies smoothly with time as in the case with two-phase flow, or when the coefficient is a deviation from a base coefficient as in the case with defects in composite materials.

We derive computable error indicators for the error introduced by refraining from recomputing a corrector after a perturbation in the coefficient. The method we propose computes all localized correctors and global stiffness matrix contributions for the first coefficient in the sequence of elliptic PDEs. For the subsequent coefficients, we use the error indicators to adaptively recompute only the correctors that need to be recomputed in order to get a sufficiently accurate solution. The coefficients that have not been recomputed we call lagging coefficients. The method is completely parallelizable over the elements on the coarse mesh. A particularly interesting setting is when only

quantities on the coarse mesh are required from the solution, for example upscaled Darcy fluxes in a Darcy flow problem, or the coarse interpolation of the full solution. Any computed fine scale quantities can then be forgotten between the iterations in the sequence and the memory requirement becomes very low.

The paper is divided into five sections: Problem formulation in Section 2, method description in Section 3, error analysis in Section 4, implementation in Section 5, and numerical experiments in Section 6. Both the method description and the error analysis are divided into four steps, with increasing level of approximation in each step: (i) reformulation by variational multiscale method (VMS), (ii) localization by LOD, (iii) approximation of localized correctors by lagging coefficient, and (iv) approximation of global stiffness matrix contribution by lagging coefficient. The main results are the methods (13) in Section 3.4, the error bound in Theorem 4 and the Algorithms 1 and 2.

2 Problem formulation

Let Ω be a polygonal domain in $\mathbb{R}^d$ (with $d = 1, 2$ or 3) with the boundary partitioned into disjoint subsets Γ_D (for Dirichlet boundary conditions) and Γ_N (for Neumann boundary conditions). Suppose we have a sequence of elliptic equations: for $n = 1, 2, \ldots$, solve for $\bar{u}^n$, such that

$$\begin{aligned} -\operatorname{div} A^n \nabla \bar{u}^n &= f && \text{in } \Omega, \\ \bar{u}^n &= g && \text{on } \Gamma_D, \\ \mathbf{n} \cdot A^n \nabla \bar{u}^n &= 0 && \text{on } \Gamma_N, \end{aligned} \tag{1}$$

where $f \in L^2(\Omega)$, $g \in H^{1/2}(\Gamma_D)$, $\mathbf{n}$ is the outward normal of the boundary, and $A^n \in L^\infty(\Omega)$ is a coefficient varying significantly over small distances. To keep the presentation short, we limit ourselves to the case where f and g are independent of n, however, the analysis in this paper can be generalized to n-dependent f and g.

As an illustrative example of the method, we will here present (and later return to) an application in this setting. Suppose we want to solve an immiscible non-capillary two-phase Darcy flow problem using the fractional flow formulation [9, 16]. This leads to a system of a coupled pressure and saturation equation

$$\begin{aligned} -\operatorname{div} \lambda(s) K \nabla u &= f, \\ \frac{\partial s}{\partial t} - \operatorname{div} \lambda_w(s) K \nabla u &= f, \end{aligned} \tag{2}$$

where space-time functions: u, s and f are pressure, saturation for the wetting phase, and sources/sinks, respectively; space function K is intrinsic permeability; and nonlinear scalar functions: λ and λ_w are total mobility and wetting phase mobility, respectively. A common technique for solving this system is sequential splitting, where the pressure equation and saturation equation are solved separately within a time step n. This means that, as we iterate in time, we need to solve a sequence of pressure equations with coefficient $A^n(x) = \lambda(s(x, t_{n-1}))K(x)$. Since the wetting saturation s changes only significantly along the plume front between time steps, we are in the setting described above.

In Sections 3 and 4, we consider a fixed time step n and drop this index for all quantities. We call the coefficient $A = A^n$ at the current time step the *true coefficient*. Ideally, only the true coefficient A would be used in the solution at the current time step. However, in order to lower the computational cost, computations from previous time steps will be reused. This means coefficients from previous time steps (*lagging coefficients*) will enter the analysis through the definition of the localized correctors and in the assembly of the global stiffness matrix. These lagging coefficients will be denoted by $\tilde{A}$. We also want to emphasize that the error indicators derived here are applicable also to situations where the coefficient deviates from a base coefficient, for example within the application of simulations of weakly random defects in composite materials.

We will work with a weak formulation of the above problem. Let $V = \{v \in H^1(\Omega) : v|_{\Gamma_D} = 0\}$. In case Γ_D is empty, we instead consider only solutions and test functions in the quotient space $V = H^1(\Omega)/\mathbb{R}$. Let $(\cdot, \cdot)$ denote the L^2-scalar product over Ω, and $(u, v)_\omega = \int_\omega uv$. Further, we define $\|v\|^2_{L^2(\omega)} = \int_\omega v^2$, $\|v\|_{L^2} = \|v\|_{L^2(\Omega)}$, and the bilinear form $a(u, v) = (A\nabla u, \nabla v)$. We let $\bar{u} = u + g$, where $u \in V$ and $g \in H^1(\Omega)$ is an extension of the boundary condition g to the full domain and seek to find $u \in V$, such that for all $v \in V$,

$$(A\nabla u, \nabla v) = (f, v) - (A\nabla g, \nabla v). \tag{3}$$

Assuming there exist constants $0 < \alpha$ and $\beta < \infty$, so that $\alpha \leq A \leq \beta$ a.e., $(A\nabla\cdot, \nabla\cdot)$ is bounded and coercive on V and existence of a unique solution is guaranteed by the Lax–Milgram theorem. We further define the energy norm $|\cdot|_A = (A\nabla\cdot, \nabla\cdot)^{1/2}$ on V, and the semi-norm $|\cdot|_{A,\omega} = (A\nabla\cdot, \nabla\cdot)^{1/2}_\omega$.

3 Method description

In this section, we describe the proposed numerical method in a series of steps, each of which introduces another level of approximation for the problem (3) above.

3.1 Variational multiscale method

The first step is to reformulate the problem using the variational multiscale method [12, 13]. This formulation forms the basis for the LOD approximation in the next section and makes it possible to reduce the dimensionality of the problem, once a corrector problem has been solved.

Let $\mathcal{T}_H$ be a regular and quasi-uniform family of conforming subdivisions of Ω into elements of maximum diameter H, and $V_H \subset V$ be a family of conforming first order finite element spaces on this mesh, e.g. $\mathcal{P}_1$ or $\mathcal{Q}_1$ depending on the shape of the elements. The choice of a linear projective quasi-interpolation operator $\mathcal{I}_H : V \to V_H$ defines the fine space as its kernel $V^{\mathrm{f}} = \ker \mathcal{I}_H = \{v \in V \,:\, \mathcal{I}_H v = 0\}$. We assume there exists a constant C independent of H so that for all $v \in V$ and $T \in \mathcal{T}_H$, it holds

$$H^{-1}\|v - \mathcal{I}_H v\|_{L^2(T)} + \|\nabla(v - \mathcal{I}_H v)\|_{L^2(T)} \leq C_{\mathcal{I}} \|\nabla v\|_{L^2(U(T))}. \tag{4}$$

Here $U(T)$ is the union of all neighboring elements to T, i.e.

$$U(T) = \bigcup \{T' \in \mathcal{T}_H \,:\, \overline{T} \cap \overline{T'} \neq \emptyset\}.$$

Since we assume $\mathcal{I}_H$ is projective (this is not strictly necessary, see e.g. [7]), we have the decomposition $V = V_H \oplus V^{\mathrm{f}}$ and can decompose the solution $u = u_H + u^{\mathrm{f}}$ and test function $v = v_H + v^{\mathrm{f}}$ and test (3) with the two spaces separately:

$$(A\nabla(u_H + u^{\mathrm{f}}), \nabla v_H) = (f, v_H) - (A\nabla g, \nabla v_H), \tag{5a}$$

$$(A\nabla u^{\mathrm{f}}, \nabla v^{\mathrm{f}}) = (f, v^{\mathrm{f}}) - (A\nabla g, \nabla v^{\mathrm{f}}) - (A\nabla u_H, \nabla v^{\mathrm{f}}). \tag{5b}$$

We note that u^{f} is linear in f and u_H, and we define the linear correction operators $\mathcal{Q} : H^1(\Omega) \to V^{\mathrm{f}}$ and $\mathcal{R} : L^2(\Omega) \to V^{\mathrm{f}}$, so that $u^{\mathrm{f}} = -\mathcal{Q}u_H + \mathcal{R}f - \mathcal{Q}g$, i.e., find $\mathcal{Q}v \in V^{\mathrm{f}}$ and $\mathcal{R}f \in V^{\mathrm{f}}$, such that for all $v^{\mathrm{f}} \in V^{\mathrm{f}}$,

$$\begin{aligned} (A\nabla \mathcal{Q}v, \nabla v^{\mathrm{f}}) &= (A\nabla v, \nabla v^{\mathrm{f}}), \\ (A\nabla \mathcal{R}f, \nabla v^{\mathrm{f}}) &= (f, v^{\mathrm{f}}). \end{aligned} \tag{6}$$

These equations have unique solutions, since $(A\nabla\cdot, \nabla\cdot)$ is still bounded and coercive on a subspace $V^{\mathrm{f}} \subset V$.

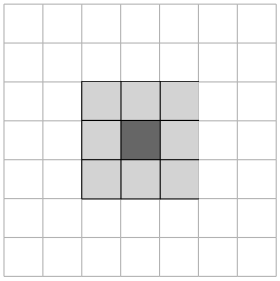

(a) One-layer element patch, $k = 1$.

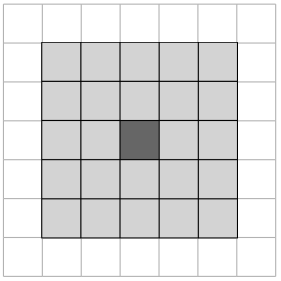

(b) Two-layer element patch, $k = 2$.

Figure 1: Illustration of k-layer element patches for quadrilateral elements. Dark gray is T. Light gray is $U_k(T)$.

We introduce a new space, the multiscale space, $V^{\mathrm{ms}} = V_H - \mathcal{Q}V_H = \{v_H - \mathcal{Q}v_H \,:\, v_H \in V_H\}$, and note that we have the orthogonality relation $V^{\mathrm{ms}} \perp_a V^{\mathrm{f}}$. The solutions $\mathcal{Q}u_H$, $\mathcal{R}f$, and $\mathcal{Q}g$ can be plugged into (5a) and we get the following low-dimensional Petrov–Galerkin problem, find $u^{\mathrm{ms}} \in V^{\mathrm{ms}}$, such that for all $v_H \in V_H$,

$$(A\nabla u^{\mathrm{ms}}, \nabla v_H) = (f, v_H) - (A\nabla g, \nabla v_H) - (A\nabla \mathcal{R}f, \nabla v_H) + (A\nabla \mathcal{Q}g, \nabla v_H). \tag{7}$$

The full solution is then $u = u^{\mathrm{ms}} + \mathcal{R}f - \mathcal{Q}g$.

Remark 1 (Right hand side correction $\mathcal{R}f$)**.** *It is possible to obtain an approximate solution even if neglecting the right hand side correction term, i.e. letting $\mathcal{R} = 0$ above. See for example [10, 15].*

3.2 Localized orthogonal decomposition

The second step is to localize the corrector computations by means of localized orthogonal decomposition (LOD). The basic idea is to solve the corrector problems (6) not globally, but on localized patches of the full domain to reduce the computational cost to compute the correctors.

For the localization, we define element patches for $T \in \mathcal{T}_H$, $U_k(T) \subset \Omega$, where $0 \leq k \in \mathbb{N}$. With trivial case $U_0(T) = T$, $U_k(T)$ (a k-layer element patch around T) is defined by the recursive relation

$$U_{k+1}(T) = \bigcup \{T' \in \mathcal{T}_H : \overline{U_k(T)} \cap \overline{T'} \neq \emptyset\}.$$

See Figure 1 for an illustration of element patches. We further define localized fine spaces

$$V^{\mathrm{f}}(U_k(T)) = \{v \in V^{\mathrm{f}} \,:\, v|_{\Omega \setminus U_k(T)} = 0\},$$

consisting of fine functions which are zero outside element patches. Throughout the paper, localized quantities are subscripted with the patch size k.

Instead of solving (6), we compute the operators $\mathcal{Q}_k = \sum_{T\in\mathcal{T}_H} \mathcal{Q}_{k,T}$ and $\mathcal{R}_k = \sum_{T\in\mathcal{T}_H} \mathcal{R}_{k,T}$, with $\mathcal{Q}_{k,T}$ and $\mathcal{R}_{k,T}$ defined by

$$\begin{aligned}(A\nabla\mathcal{Q}_{k,T}v, \nabla v^{\mathrm{f}}) &= (A\nabla v, \nabla v^{\mathrm{f}})_T,\\ (A\nabla\mathcal{R}_{k,T}f, \nabla v^{\mathrm{f}}) &= (f, v^{\mathrm{f}})_T,\end{aligned} \tag{8}$$

for all $v^{\mathrm{f}} \in V^{\mathrm{f}}(U_k(T))$ and all $T \in \mathcal{T}_H$.

We define the localized multiscale space $V_k^{\mathrm{ms}} = V_H - \mathcal{Q}_k V_H$. Our localized multiscale problem reads find $u_k^{\mathrm{ms}} \in V_k^{\mathrm{ms}}$, such that for all $v_H \in V_H$,

$$\begin{aligned}(A\nabla u_k^{\mathrm{ms}}, \nabla v_H) = (f, v_H) - (A\nabla g, \nabla v_H) - \\ (A\nabla\mathcal{R}_k f, \nabla v_H) + (A\nabla\mathcal{Q}_k g, \nabla v_H),\end{aligned}$$

and the full solution for the second approximation is $u_k = u_k^{\mathrm{ms}} + \mathcal{R}_k f - \mathcal{Q}_k g$.

3.3 Lagging multiscale space

In the third approximation we compute the localized element correctors using a lagging coefficient $\tilde{A}_T$ rather than the true A. This makes it possible to reuse correctors that have been computed at earlier time steps, so that localized correctors only for a small number of elements T need to be recomputed.

We define the lagging localized corrector operators $\tilde{\mathcal{Q}}_k = \sum_T \tilde{\mathcal{Q}}_{k,T}$ and $\tilde{\mathcal{R}}_k = \sum_T \tilde{\mathcal{R}}_{k,T}$. The element corrector operators $\tilde{\mathcal{Q}}_{k,T}v, \tilde{\mathcal{R}}_{k,T}f \in V^{\mathrm{f}}(U_k(T))$ are defined such that for all $v^{\mathrm{f}} \in V^{\mathrm{f}}(U_k(T))$,

$$\begin{aligned}(\tilde{A}_T\nabla\tilde{\mathcal{Q}}_{k,T}v, \nabla v^{\mathrm{f}}) &= (\tilde{A}_T\nabla v, \nabla v^{\mathrm{f}})_T,\\ (\tilde{A}_T\nabla\tilde{\mathcal{R}}_{k,T}f, \nabla v^{\mathrm{f}}) &= (f, v^{\mathrm{f}})_T.\end{aligned} \tag{9}$$

Note that lagging coefficients $\tilde{A}_T$ are not necessarily the same for all T.

Example 1 (Relation between lagging coefficient and time steps)**.** *As an example, for the current time step $A = A^n$, for element T' the coefficient can be one time step old, i.e. $\tilde{A}_{T'} = A^{n-1}$ and for T'' three time steps old, i.e. $\tilde{A}_{T''} = A^{n-3}$. That is, different lagging localized element correctors may be defined in terms of coefficients from different time steps in history.*

In analogy with previous multiscale spaces, we define a lagging multiscale space $\tilde{V}_k^{\mathrm{ms}} = V_H - \tilde{\mathcal{Q}}_k V_H$ and the problem is then to find $\tilde{u}_k^{\mathrm{ms}} \in \tilde{V}_k^{\mathrm{ms}}$, such that for all $v_H \in V_H$,

$$(A\nabla\tilde{u}_k^{\mathrm{ms}}, \nabla v_H) = (f, v_H) - (A\nabla g, \nabla v_H) - (A\nabla\tilde{\mathcal{R}}_k f, \nabla v_H) + (A\nabla\tilde{\mathcal{Q}}_k g, \nabla v_H) \tag{10}$$

and the full solution for the third approximation is $\tilde{u}_k = \tilde{u}_k^{\mathrm{ms}} + \tilde{\mathcal{R}}_k f - \tilde{\mathcal{Q}}_k g$.

3.4 Lagging global stiffness matrix contribution

The fourth approximation involves not only using a lagging multiscale space, but also a lagging coefficient in the assembly of the global stiffness matrix and right hand side. The rationale behind this is that computing the integrals in the stiffness matrix and right hand side for (10) requires that all precomputed element correctors are stored. To circumvent this, we propose the following approximation. First we define a lagging bilinear form $\tilde{a}$ (and its elementwise contributor $\tilde{a}_T$), based on the same lagging coefficients $\tilde{A}_T$ as was used for the multiscale space in the previous section,

$$\tilde{a}(u,v) := \sum_{T\in\mathcal{T}_H} \tilde{a}_T(u,v) := \sum_{T\in\mathcal{T}_H} (\tilde{A}_T(\chi_T\nabla - \nabla\tilde{\mathcal{Q}}_{k,T})\mathcal{I}_H u, \nabla v) \tag{11}$$

where χ_T is the indicator function for subset $T \subset \Omega$. We also define a lagging linear functional $\tilde{L}$ (and its elementwise contributor $\tilde{L}_T$),

$$\begin{aligned}\tilde{L}(v) &:= \sum_{T\in\mathcal{T}_H} \tilde{L}_T(v) \\ &:= \sum_{T\in\mathcal{T}_H} (f,v)_T - (A\nabla g, \nabla v)_T - (\tilde{A}_T\nabla\tilde{\mathcal{R}}_{k,T}f, \nabla v) + (\tilde{A}_T\nabla\tilde{\mathcal{Q}}_{k,T}g, \nabla v).\end{aligned} \tag{12}$$

Then the problem is posed as to find $\hat{u}_k^{\text{ms}} \in \tilde{V}_k^{\text{ms}}$, such that for all $v_H \in V_H$,

$$\tilde{a}(\hat{u}_k^{\text{ms}}, v_H) = \tilde{L}(v_H). \tag{13}$$

The full solution for the final approximation step is then $\hat{u}_k = \hat{u}_k^{\text{ms}} + \tilde{\mathcal{R}}_k f - \tilde{\mathcal{Q}}_k g$.

We note that (13) coincides with (10) when $\tilde{A}_T = A$ for all T. Also, we note that the coefficients for the linear system can be computed immediately after $\tilde{\mathcal{Q}}_{k,T}$ and $\tilde{\mathcal{R}}_{k,T}$ have been computed. This means no correctors need to exist simultaneously.

This method is independent of the true coefficient A, if not $\tilde{A}_T = A$ for any T. In order to construct a numerical method with control of the error from this approximation, we use error indicators on the element correctors to determine whether they need to be recomputed or not. Next, we define three computable error indicators, e_u, e_f and e_g, for the error introduced by using a lagging coefficient.

3.5 Error indicators

As can be seen in later Sections 4.3 and 4.4, the differences $|\mathcal{Q}_{k,T}v - \tilde{\mathcal{Q}}_{k,T}v|_A$ for $v \in V_H$, $|\mathcal{R}_{k,T}f - \tilde{\mathcal{R}}_{k,T}f|_A$, and $|\mathcal{Q}_{k,T}g - \tilde{\mathcal{Q}}_{k,T}g|_A$ constitute the sources to

the error in the approximation from using lagging coefficients. In this section, we define three elementwise error indicators ($e_{u,T}$, $e_{f,T}$, and $e_{g,T}$) and relate them to the above differences in Lemma 2.

Lemma 2 (Error indicators: definitions and bounds)**.** *The following bounds hold,*

$$\begin{aligned}
|\mathcal{Q}_{k,T}v - \tilde{\mathcal{Q}}_{k,T}v|_A &\le e_{u,T}|v|_{A,T}, \qquad \text{for all } v \in V_H,\\
|\mathcal{R}_{k,T}f - \tilde{\mathcal{R}}_{k,T}f|_A &\le e_{f,T}\|f\|_{L^2(T)},\\
|\mathcal{Q}_{k,T}g - \tilde{\mathcal{Q}}_{k,T}g|_A &\le e_{g,T}|g|_{A,T},
\end{aligned}$$

where

$$\begin{aligned}
e_{u,T} &= \max_{w|_T\,:\,w\in V_H, |w|_{A,T}=1} \|(\tilde{A}_T - A)A^{-1/2}(\chi_T\nabla w - \nabla\tilde{\mathcal{Q}}_{k,T}w)\|_{L^2(U_k(T))},\\
e_{f,T} &= \frac{\|(\tilde{A}_T - A)A^{-1/2}\nabla\tilde{\mathcal{R}}_{k,T}f\|_{L^2(U_k(T))}}{\|f\|_{L^2(T)}} \qquad \text{or 0 if } \|f\|_{L^2(T)} = 0,\\
e_{g,T} &= \frac{\|(\tilde{A}_T - A)A^{-1/2}(\chi_T\nabla g - \nabla\tilde{\mathcal{Q}}_{k,T}g)\|_{L^2(U_k(T))}}{|g|_{A,T}} \qquad \text{or 0 if } |g|_{A,T} = 0.
\end{aligned}$$

We additionally define

$$e_u = \max_{T\in\mathcal{T}_H} e_{u,T}, \quad e_f = \max_{T\in\mathcal{T}_H} e_{f,T}, \quad \text{and } e_g = \max_{T\in\mathcal{T}_H} e_{g,T}.$$

Proof. For any $v \in V_H$, let $z = \mathcal{Q}_{k,T}v - \tilde{\mathcal{Q}}_{k,T}v$, then using (8) and (9), we get

$$\begin{aligned}
|z|^2_{A,U_k(T)} &= (A\nabla(\mathcal{Q}_{k,T}v - \tilde{\mathcal{Q}}_{k,T}v), \nabla z)_{U_k(T)}\\
&= ((\tilde{A}_T - A)\nabla\tilde{\mathcal{Q}}_{k,T}v, \nabla z)_{U_k(T)} - ((\tilde{A}_T - A)\nabla v, \nabla z)_T\\
&\le \|(\tilde{A}_T - A)A^{-1/2}(\chi_T\nabla v - \nabla\tilde{\mathcal{Q}}_{k,T}v)\|_{L^2(U_k(T))}\cdot|z|_{A,U_k(T)}.
\end{aligned}$$

Then, clearly $e_{u,T}$ (if it exists) constitute the asserted bound. The following inequality gives a bound for the norm being maximized in the definition of $e_{u,T}$ (assuming that $|w|_{A,T} = 1$),

$$\begin{aligned}
&\|(\tilde{A}_T - A)A^{-1/2}(\chi_T\nabla w - \nabla\tilde{\mathcal{Q}}_{k,T}w)\|_{L^2(U_k(T))}\\
&\quad\le \|(\tilde{A}_T - A)A^{-1}\|_{L^\infty(T)} +\\
&\qquad \|(\tilde{A}_T - A)A^{-1/2}\tilde{A}_T^{-1/2}\|_{L^\infty(U_k(T))}\|A^{-1/2}\tilde{A}_T^{1/2}\|_{L^\infty(T)}.
\end{aligned}$$

The maximum is thus attained and exists by the extreme value theorem.

Similarly, for $z = \mathcal{R}_{k,T}f - \tilde{\mathcal{R}}_{k,T}f$, we have

$$\begin{aligned}
|z|^2_{A,U_k(T)} &= (A\nabla(\mathcal{R}_{k,T}f - \tilde{\mathcal{R}}_{k,T}f), \nabla z)_{U_k(T)}\\
&= ((\tilde{A}_T - A)\nabla\tilde{\mathcal{R}}_{k,T}f, \nabla z)_{U_k(T)}\\
&\le \|(\tilde{A}_T - A)A^{-1/2}\nabla\tilde{\mathcal{R}}_{k,T}f\|_{L^2(U_k(T))}\cdot|z|_{A,U_k(T)},
\end{aligned}$$

which motivates the definition of $e_{f,T}$ and the asserted bound. The result for $e_{g,T}$ holds analogously. □

Regarding the computation of these error indicators, both $e_{f,T}$ and $e_{g,T}$ are straight-forward to compute, being a ratio of two computable norms. The error indicator $e_{u,T}$ is also easy to compute. It is the square root of a Rayleigh quotient for a generalized eigenvalue problem (where the restriction $|w|_{A,T} = 1$ removes the singularity of the denominator matrix):

$$\mathbf{B}\mathbf{x}_\ell = \mu_\ell \mathbf{C}\mathbf{x}_\ell$$

with the matrices

$$B_{ij} = \big((\tilde{A}_T - A)^2 A^{-1}(\chi_T \nabla\phi_j - \nabla\tilde{\mathcal{Q}}_{k,T}\phi_j), \chi_T\nabla\phi_i - \nabla\tilde{\mathcal{Q}}_{k,T}\phi_i\big)_{U_k(T)},$$
$$C_{ij} = (A\nabla\phi_j, \nabla\phi_i)_T,$$

for all $i, j = 1, \ldots, m-1$ where m is the number of basis functions in T (i.e. one of them removed). The squared maximum $e_{u,T}^2$ corresponds to the maximum eigenvalue $\max_\ell \mu_\ell$. We emphasize that the matrices $\mathbf{B}$ and $\mathbf{C}$ are very small: the same size as the number of degrees of freedom in the coarse element T (minus one for removing the constant), e.g., 2×2 for 2D simplicial meshes or 7×7 for 3D hexahedral meshes.

3.5.1 Coarse error indicators

In order to compute the error indicators $e_{u,T}$, $e_{f,T}$, and $e_{g,T}$ we need access to the true coefficient A and lagging correctors $\tilde{\mathcal{Q}}_{k,T}\phi_i$, $\tilde{\mathcal{R}}_{k,T}f$, and $\tilde{\mathcal{Q}}_{k,T}g$ at the same time. This implies all lagging correctors need to be saved in order to compute the error indicators. Since the correctors in practice are defined on patches of a fine mesh, and the patch overlap can be substantial, the memory requirements for saving them might be large. In this section, we construct an additional bound that makes it possible to discard the lagging correctors after they have been computed.

We construct the following bound starting from the definition of $e_{u,T}$ in

Lemma 2,

$$\begin{aligned} e_{u,T}^2 &\leq \sum_{\substack{T'\in\mathcal{T}_H\\ T'\cap U_k(T)\neq\emptyset}} \max_{\substack{w|_T\,:\,w\in V_H,\\ |w|_{A,T}=1}} \|(\tilde{A}_T - A)A^{-1/2}(\chi_T\nabla w - \nabla\tilde{\mathcal{Q}}_{k,T}w)\|^2_{L^2(T')} \\ &\leq \sum_{\substack{T'\in\mathcal{T}_H\\ T'\cap U_k(T)\neq\emptyset}} \|\delta_T\|^2_{L^\infty(T')}\|A^{-1/2}\tilde{A}_T^{1/2}\|^2_{L^\infty(T)}\cdot \\ &\qquad\qquad \cdot \max_{\substack{w|_T\,:\,w\in V_H,\\ |w|_{\tilde{A}_T,T}=1}} \|\tilde{A}_T^{1/2}(\chi_T\nabla w - \nabla\tilde{\mathcal{Q}}_{k,T}w)\|^2_{L^2(T')} \\ &=: E_{u,T}. \end{aligned} \tag{14}$$

where $\delta_T = (\tilde{A}_T - A)A^{-1/2}\tilde{A}_T^{-1/2}$, and we used that

$$|w|_{\tilde{A}_T,T} \leq \|A^{-1/2}\tilde{A}_T^{1/2}\|_{L^\infty(T)}|w|_{A,T}$$

in the last inequality. We further define $E_u = \max_{T\in\mathcal{T}_H} E_{u,T}$.

The maximum in (14) corresponds to a maximum eigenvalue of a low-dimensional generalized eigenvalue problem, as was the case for $e_{u,T}$ in Section 3.5. More specifically, it is the square root of the maximum eigenvalue

$$\tilde{\mu}_{T,T'} := \max_\ell \mu_\ell \tag{15}$$

of $\mathbf{B}\mathbf{x}_\ell = \mu_\ell\mathbf{C}\mathbf{x}_\ell$ with the matrices

$$\begin{aligned} B_{ij} &= \big(\tilde{A}_T(\chi_T\nabla\phi_j - \nabla\tilde{\mathcal{Q}}_{k,T}\phi_j), \chi_T\nabla\phi_i - \nabla\tilde{\mathcal{Q}}_{k,T}\phi_i\big)_{T'}, \\ C_{ij} &= (\tilde{A}_T\nabla\phi_j, \nabla\phi_i)_T, \end{aligned}$$

for $i,j = 1,\ldots,m-1$, where m is the number of basis functions in T. We note that the quantity $\tilde{\mu}_{T,T'}$ can be computed directly after corrector $\tilde{\mathcal{Q}}_{k,T}$ has been computed for the basis functions in element T. Now, $\tilde{\mathcal{Q}}_{k,T}$ does not need to be saved for computing $E_{u,T}$ later, and it can be discarded. In particular, the memory required for storing $\tilde{\mu}_{T,T'}$ (which, however, is needed to compute $E_{u,T}$) scales like $\mathcal{O}(k^dH^{-d})$.

Still, $\tilde{A}_T$ needs to be available to compute $\|A^{-1/2}\tilde{A}_T^{1/2}\|^2_{L^\infty(T)}$ and δ_T. This might not be a problem in applications where there is a low-dimensional description of the coefficient, for example if the coefficient is defined by a set of geometric shapes which can be described by location, size, shape and so on. In the application of two-phase Darcy flow, we will return to a way to avoid saving $\tilde{A}_T$ in Section 5.2.2.

The error indicator E_u can replace e_u in all results and algorithms in this work. Similar coarse error indicators can be derived for e_f and e_g.

4 Error analysis

In this section we study the approximation error of the three approximations u_k, $\tilde{u}_k$ and $\hat{u}_k$, and the inf-sup stability for the systems yielding the solutions u^{ms}, u_k^{ms}, $\tilde{u}_k^{\mathrm{ms}}$ and $\hat{u}_k^{\mathrm{ms}}$. Finally, in Theorem 4 in Section 4.4, we present a bound on the error $u - \hat{u}_k$ of the full approximation.

We use C to denote a constant that is independent of the regularity of u, patch size k and coarse mesh size H. It can, however, depend on the contrast $\frac{\beta}{\alpha}$. The value of the constant is not tracked between steps in inequalities. By the notation $a \lesssim b$, we mean $a \leq Cb$.

4.1 Variational multiscale method

Since the varitional multiscale formulation (7) is only a reformulation of the original problem, without any approximations, there is no error. However, the well-posedness of the formulation is still of interest.

4.1.1 Stability

Uniqueness of a solution to (7) is guaranteed by an inf-sup condition for a on V^{ms} and V_H,

$$\begin{aligned}
\inf_{w\in V^{\mathrm{ms}}}\sup_{v\in V_H}\frac{|(A\nabla w,\nabla v)|}{|w|_A|v|_A} &= \inf_{w\in V_H}\sup_{v\in V_H}\frac{|(A\nabla(w-\mathcal{Q}w),\nabla v)|}{|w-\mathcal{Q}w|_A|v|_A}\\
&= \inf_{w\in V_H}\sup_{v\in V_H}\frac{|(A\nabla(w-\mathcal{Q}w),\nabla(v-\mathcal{Q}v))|}{|w-\mathcal{Q}w|_A|v|_A}\\
&\geq \inf_{w\in V_H}\frac{|w-\mathcal{Q}w|_A^2}{|w-\mathcal{Q}w|_A|w|_A}\\
&= \inf_{w\in V_H}\frac{|w-\mathcal{Q}w|_A^2}{|w-\mathcal{Q}w|_A|\mathcal{I}_H(w-\mathcal{Q}w)|_A}\\
&\geq C_{\mathcal{I}}^{-1}\alpha^{1/2}\beta^{-1/2} =: \gamma.
\end{aligned}$$

The existence inf-sup condition holds analogously. We let γ denote the inf-sup stability constant and note that it is depends on the contrast for general $\mathcal{I}_H$. See [8, 19] for corrector localization results independent of the contrast.

4.2 Localized orthogonal decomposition

For the error analysis of LOD we recite previous exponential decay results (first presented in [15]) of the localized corrector operators by means of the

following lemmas. For example, the proof in [10, Lemma 3.6] is almost directly applicable here.

Lemma 3 (Localization error)**.** *Let $k > 0$ be a fixed integer and let $p_T \in V^{\mathrm{f}}$ be the solution of*

$$(A\nabla p_T, \nabla v^{\mathrm{f}}) = F_T(v^{\mathrm{f}})$$

for all $v^{\mathrm{f}} \in V^{\mathrm{f}}$, where $F_T \in V^*$ such that $F_T(v^{\mathrm{f}}) = 0$ for all $v^{\mathrm{f}} \in V^{\mathrm{f}}(\Omega \setminus T)$. Furthermore, we let $p_{k,T} \in V^{\mathrm{f}}(U_k(T))$ be the solution of

$$(A\nabla p_{k,T}, \nabla v^{\mathrm{f}}) = F_T(v^{\mathrm{f}})$$

for all $v^{\mathrm{f}} \in V^{\mathrm{f}}(U_k(T))$. Then there exists a constant $0 < \theta < 1$ that depends on the contrast but not on H or the variations of A, such that

$$\left| \sum_T p_T - p_{k,T} \right|_A^2 \lesssim k^d \theta^{2k} \sum_T |p_T|_A^2 .$$

This lemma can be applied for the localization error of both $\mathcal{Q} - \mathcal{Q}_k$ and $\mathcal{R} - \mathcal{R}_k$. In analogy with the definition of $\mathcal{Q}_k$ as a sum of $\mathcal{Q}_{k,T}$, we can define $\mathcal{Q} = \sum_{T \in \mathcal{T}_H} \mathcal{Q}_T$ with $\mathcal{Q}_T = \mathcal{Q}_{\infty,T}$. Then for any $v \in V$, we can identify $\mathcal{Q}_T v$ with p_T and $\mathcal{Q}_{k,T} v$ with $p_{k,T}$ in the lemma above (and similarly for $\mathcal{R}$).

4.2.1 Stability

Using Lemma 3, we get the following result for $\mathcal{Q}v - \mathcal{Q}_k v$, with $v \in H^1(\Omega)$,

$$|\mathcal{Q}v - \mathcal{Q}_k v|_A^2 \lesssim k^d \theta^{2k} \sum_T |\mathcal{Q}_T v|_A^2 \lesssim k^d \theta^{2k} |v|_A^2. \tag{16}$$

If in addtion $v \in V_H$, we can use the stability of $\mathcal{I}_H$ and continue to get

$$|v|_A^2 \lesssim |\mathcal{I}_H(v - \mathcal{Q}v)|_A^2 \lesssim |v - \mathcal{Q}v|_A^2.$$

Using the result above, we can derive an inf-sup constant for a and the pair of spaces V_k^{ms} and V_H,

$$\begin{aligned}
&\inf_{w_k^{\mathrm{ms}} \in V_k^{\mathrm{ms}}} \sup_{v \in V_H} \frac{|a(w_k^{\mathrm{ms}}, v)|}{|w_k^{\mathrm{ms}}|_A |v|_A} \\
&\quad \geq \inf_{w \in V_H} \sup_{v \in V_H} \frac{|a(w - \mathcal{Q}w, v)| - |a(\mathcal{Q}w - \mathcal{Q}_k w, v)|}{(|w - \mathcal{Q}w|_A + |\mathcal{Q}w - \mathcal{Q}_k w|_A)|v|_A} \\
&\quad \geq \inf_{w \in V_H} \sup_{v \in V_H} \frac{|a(w - \mathcal{Q}w, v)| - Ck^{d/2}\theta^k |w - \mathcal{Q}w|_A |v|_A}{(1 + Ck^{d/2}\theta^k)|w - \mathcal{Q}w|_A |v|_A} \\
&\quad \geq \frac{\gamma - Ck^{d/2}\theta^k}{1 + Ck^{d/2}\theta^k} =: \gamma_k.
\end{aligned} \tag{17}$$

For sufficiently large k, there is a uniform bound $\gamma_0 \leq \gamma_k$. See [7] for more details on stability of this approximation.

4.2.2 Error

For arbitrary $u_I \in V_k^{\text{ms}}$, using the equations (7) and (8), we have for all $v \in V_H$,

$$\begin{aligned}(A\nabla(u_k^{\text{ms}} - u_I), \nabla v) = (A\nabla(u^{\text{ms}} - u_I), \nabla v) + \\ (A\nabla(\mathcal{R}f - \mathcal{R}_k f), \nabla v) - (A\nabla(\mathcal{Q}g - \mathcal{Q}_k g), \nabla v).\end{aligned}$$

The inf-sup condition for uniqueness above yields the following approximation result, for arbitrary $u_I \in V_k^{\text{ms}}$,

$$\gamma_0 |u_k^{\text{ms}} - u_I|_A \leq |u^{\text{ms}} - u_I|_A + |\mathcal{R}f - \mathcal{R}_k f|_A + |\mathcal{Q}g - \mathcal{Q}_k g|_A.$$

In analogy with (16) we get the following result for $\mathcal{R}f - \mathcal{R}_k f$,

$$|\mathcal{R}f - \mathcal{R}_k f|_A^2 \lesssim k^d \theta^{2k} \sum_T |\mathcal{R}_T f|_A^2 \lesssim k^d \theta^{2k} \|f\|_{L^2}^2.$$

Recall that $u = \mathcal{I}_H u^{\text{ms}} - \mathcal{Q}\mathcal{I}_H u^{\text{ms}} + \mathcal{R}f - \mathcal{Q}g$ and $u_k = \mathcal{I}_H u_k^{\text{ms}} - \mathcal{Q}_k \mathcal{I}_H u_k^{\text{ms}} + \mathcal{R}_k f - \mathcal{Q}_k g$. Now, if we choose $u_I = \mathcal{I}_H u^{\text{ms}} - \mathcal{Q}_k \mathcal{I}_H u^{\text{ms}} \in V_k^{\text{ms}}$, then $u^{\text{ms}} - u_I = -(\mathcal{Q} - \mathcal{Q}_k)\mathcal{I}_H u^{\text{ms}}$ and using the approximation result we get

$$\begin{aligned}&|u^{\text{ms}} - u_k^{\text{ms}}|_A \\ &\quad \leq |u^{\text{ms}} - u_I|_A + |u_k^{\text{ms}} - u_I|_A \\ &\quad \leq (1 + \gamma_0^{-1})|u^{\text{ms}} - u_I|_A + \gamma_0^{-1}(|\mathcal{R}f - \mathcal{R}_k f|_A + |\mathcal{Q}g - \mathcal{Q}_k g|_A) \\ &\quad \leq (1 + \gamma_0^{-1})|(\mathcal{Q} - \mathcal{Q}_k)\mathcal{I}_H u^{\text{ms}}|_A + \gamma_0^{-1}(|\mathcal{R}f - \mathcal{R}_k f|_A + |\mathcal{Q}g - \mathcal{Q}_k g|_A).\end{aligned} \tag{18}$$

Then, using $\mathcal{I}_H u^{\text{ms}} = \mathcal{I}_H u$, interpolation stability (4) and stability of the continuous problem, we have for the full error

$$\begin{aligned}|u - u_k|_A &\leq |u^{\text{ms}} - u_k^{\text{ms}}|_A + |(\mathcal{R} - \mathcal{R}_k)f|_A + |(\mathcal{Q} - \mathcal{Q}_k)g|_A \\ &\leq (1 + \gamma_0^{-1})\left(|(\mathcal{Q} - \mathcal{Q}_k)\mathcal{I}_H u^{\text{ms}}|_A + |\mathcal{R}f - \mathcal{R}_k f|_A - |\mathcal{Q}g - \mathcal{Q}_k g|_A\right) \\ &\lesssim (1 + \gamma_0^{-1}) k^{d/2} \theta^k \left(|\mathcal{I}_H u^{\text{ms}}|_A + \|f\|_{L^2} + |g|_A\right) \\ &\lesssim (1 + \gamma_0^{-1}) k^{d/2} \theta^k \left(|u|_A + \|f\|_{L^2} + |g|_A\right) \\ &\lesssim (1 + \gamma_0^{-1}) k^{d/2} \theta^k (\|f\|_{L^2} + |g|_A).\end{aligned} \tag{19}$$

This result was first shown in [15] and is noteworthy, since the error of the approximation decays exponentially with increasing k, independently of the regularity of the solution u.

4.3 Lagging multiscale space

For this step, we use a lagging multiscale space $\tilde{V}_k^{\mathrm{ms}}$ and need to establish an inf-sup stability constant for a with respect to $\tilde{V}_k^{\mathrm{ms}}$ and V_H. We will use the results from Lemma 2 both for deriving stability and the approximation error. The following full corrector error can be derived using Lemma 2,

$$\begin{aligned} |\mathcal{Q}_k w - \tilde{\mathcal{Q}}_k w|_A^2 &= \Big| \sum_T (\mathcal{Q}_{k,T} w - \tilde{\mathcal{Q}}_{k,T} w) \Big|_A^2 \\ &\lesssim k^d \sum_T |\mathcal{Q}_{k,T} w - \tilde{\mathcal{Q}}_{k,T} w|_{A,U_k(T)}^2 \\ &\leq k^d e_u^2 |w|_A^2. \end{aligned} \tag{20}$$

The bounds $|\mathcal{R}_k f - \tilde{\mathcal{R}}_k f|_A^2 \lesssim k^d e_f^2 \|f\|_{L^2}^2$ and $|\mathcal{Q}_k g - \tilde{\mathcal{Q}}_k g|_A^2 \lesssim k^d e_g^2 |g|_A^2$ hold similarly.

We note that if $\tilde{A}_T = A$, then $e_{u,T} = e_{f,T} = e_{g,T} = 0$. Obviously, updating a lagging coefficient for an element corrector leads to no error for this element corrector.

4.3.1 Stability

We can now derive an inf-sup constant for a on $\tilde{V}_k^{\mathrm{ms}}$ and V_H, using similar techniques as in (17),

$$\begin{aligned} &\inf_{\tilde{w}_k^{\mathrm{ms}} \in \tilde{V}_k^{\mathrm{ms}}} \sup_{v \in V_H} \frac{|a(\tilde{w}_k^{\mathrm{ms}}, v)|}{|\tilde{w}_k^{\mathrm{ms}}|_A |v|_A} \\ &\quad \geq \inf_{w \in V_H} \sup_{v \in V_H} \frac{|a(w - \mathcal{Q}_k w, v)| - |a(\mathcal{Q}_k w - \tilde{\mathcal{Q}}_k w, v)|}{(|w - \mathcal{Q}_k w|_A + |\mathcal{Q}_k w - \tilde{\mathcal{Q}}_k w|_A)|v|_A} \\ &\quad \geq \inf_{w \in V_H} \sup_{v \in V_H} \frac{|a(w - \mathcal{Q}_k w, v)| - C k^{d/2} e_u |w - \mathcal{Q} w|_A |v|_A}{(1 + C k^{d/2} e_u)|w - \mathcal{Q}_k w|_A |v|_A} \\ &\quad \geq \frac{\gamma_k - C k^{d/2} e_u}{1 + C k^{d/2} e_u} =: \tilde{\gamma}_k. \end{aligned}$$

We note that k enters the constant, but that it can be compensated by a small e_u. Since $e_{u,T}$ is computable, a rule to recompute all element correctors T with $e_{u,T} \geq \mathrm{TOL}(k)$ for some small enough $\mathrm{TOL}(k) = \mathcal{O}(k^{-d/2})$, will (after recomputation) make $\tilde{A}_T = A$ and $e_{u,T} = 0$. This makes $e_u < \mathrm{TOL}(k)$. Following this adaptive rule makes it possible to find a lower bound $\tilde{\gamma}_0 \leq \tilde{\gamma}_k$ for sufficiently large k and sufficiently small TOL.

4.3.2 Error

Again, we get an approximation result from the inf-sup stability. In complete analogy with (18) and (19), we get

$$\begin{aligned}
&|u_k - \tilde{u}_k|_A \\
&\quad \leq (1+\tilde{\gamma}_0^{-1}) \left(|(\mathcal{Q}_k - \tilde{\mathcal{Q}}_k)\mathcal{I}_H u_k^{\mathrm{ms}}|_A + |\mathcal{R}_k f - \tilde{\mathcal{R}}_k f|_A + |\mathcal{Q}_k g - \tilde{\mathcal{Q}}_k g|_A \right) \\
&\quad \lesssim (1+\tilde{\gamma}_0^{-1}) k^{d/2} \left(e_u |u_k|_A + e_f \|f\|_{L^2} + e_g |g|_A \right) \\
&\quad \lesssim (1+\tilde{\gamma}_0^{-1}) \gamma_0^{-1} k^{d/2} \max(e_u, e_f, e_g) (\|f\|_{L^2} + |g|_A).
\end{aligned} \tag{21}$$

4.4 Lagging global stiffness matrix contribution

In the fourth approximation (13), the coefficients for the integration of the global stiffness matrix and (parts of) the right hand side are also lagging.

4.4.1 Stability

We derive an inf-sup constant for $\tilde{a}$ (see (11)) with respect to $\tilde{V}_k^{\mathrm{ms}}$ and V_H,

$$\begin{aligned}
&\inf_{\tilde{w}_k^{\mathrm{ms}} \in \tilde{V}_k^{\mathrm{ms}}} \sup_{v \in V_H} \frac{|\tilde{a}(\tilde{w}_k^{\mathrm{ms}}, v)|}{|\tilde{w}_k^{\mathrm{ms}}|_A |v|_A} \\
&\quad \geq \inf_{\tilde{w}_k^{\mathrm{ms}} \in \tilde{V}_k^{\mathrm{ms}}} \sup_{v \in V_H} (|\tilde{w}_k^{\mathrm{ms}}|_A |v|_A)^{-1} \Big(|a(\tilde{w}_k^{\mathrm{ms}}, v)| - \\
&\qquad \Big| \sum_{T \in \mathcal{T}_H} \int_{U_k(T)} (\tilde{A}_T - A)(\chi_T \nabla - \nabla \tilde{\mathcal{Q}}_{k,T}) \mathcal{I}_H \tilde{w}_k^{\mathrm{ms}} \cdot \nabla v \Big| \Big) \\
&\quad \geq \tilde{\gamma}_k - \inf_{w \in V_H} \sup_{v \in V_H} \frac{\sum_T e_{u,T} \|A^{1/2} \nabla w\|_{L^2(T)} \|A^{1/2} \nabla v\|_{L^2(U_k(T))}}{|w - \tilde{\mathcal{Q}}_k w|_A |v|_A} \\
&\quad \geq \tilde{\gamma}_k - \inf_{w \in V_H} \frac{C k^{d/2} e_u \|A^{1/2} \nabla w\|_{L^2}}{|w - \tilde{\mathcal{Q}}_k w|_A} \\
&\quad = \tilde{\gamma}_k - \inf_{w \in V_H} \frac{C k^{d/2} e_u \|A^{1/2} \nabla \mathcal{I}_H (w - \tilde{\mathcal{Q}}_k w)\|_{L^2}}{|w - \tilde{\mathcal{Q}}_k w|_A} \\
&\quad \geq \tilde{\gamma}_k - C k^{d/2} e_u =: \hat{\gamma}_k
\end{aligned}$$

Again, k enters, but can be compensated by a small e_u according to the discussion in Section 4.3.1. Thus, there is a bound $\hat{\gamma}_0 \leq \hat{\gamma}_k$ for all sufficiently large k.

4.4.2 Error

To study the error $|\tilde{u}_k - \hat{u}_k|_A$, we first note that $|\tilde{u}_k - \hat{u}_k|_A = |\tilde{u}_k^{\text{ms}} - \hat{u}_k^{\text{ms}}|_A$, since the right hand side and boundary condition corrections are the same in both cases. We form the following difference from (10) and (13),

$$\begin{aligned} &a(\tilde{u}_k^{\text{ms}}, v_H) - \tilde{a}(\hat{u}_k^{\text{ms}}, v_H) \\ &\quad = \sum_T ((\tilde{A}_T - A)\nabla\tilde{\mathcal{R}}_{k,T} f, \nabla v_H) - \sum_T ((\tilde{A}_T - A)\nabla\tilde{\mathcal{Q}}_{k,T} g, \nabla v_H). \end{aligned} \tag{22}$$

Add and subtract $a(\hat{u}_k^{\text{ms}}, v_H)$ and use Lemma 2 to get

$$\begin{aligned} &|a(\tilde{u}_k^{\text{ms}} - \hat{u}_k^{\text{ms}}, v_H)| \\ &\quad = \Big| \sum_T ((\tilde{A}_T - A)(\chi_T\nabla - \nabla\tilde{\mathcal{Q}}_{k,T})\mathcal{I}_H\hat{u}_k^{\text{ms}}, \nabla v_H) + \\ &\qquad \sum_T ((\tilde{A}_T - A)\nabla\tilde{\mathcal{R}}_{k,T} f, \nabla v_H) - \\ &\qquad \sum_T ((\tilde{A}_T - A)\nabla\tilde{\mathcal{Q}}_{k,T} g, \nabla v_H)\Big| \\ &\quad \leq \sum_T \Big(\|(\tilde{A}_T - A)A^{-1/2}(\chi_T\nabla - \nabla\tilde{\mathcal{Q}}_{k,T})\mathcal{I}_H\hat{u}_k^{\text{ms}}\|_{L^2(U_k(T))} + \\ &\qquad\qquad \|(\tilde{A}_T - A)A^{-1/2}\nabla\tilde{\mathcal{R}}_{k,T} f\|_{L^2(U_k(T))} + \\ &\qquad\qquad \|(\tilde{A}_T - A)A^{-1/2}\nabla\tilde{\mathcal{Q}}_{k,T} g\|_{L^2(U_k(T))}\Big) |v_H|_{A,U_k(T)} \\ &\quad \lesssim k^{d/2}\Big(\sum_T e_{u,T}^2 |\mathcal{I}_H\hat{u}_k^{\text{ms}}|_{A,T}^2 + e_{f,T}^2\|f\|_{L^2(T)}^2 + e_{g,T}^2|g|_{A,T}\Big)^{1/2} |v_H|_A \\ &\quad \leq k^{d/2}\max(e_u, e_f, e_g)\big(|\mathcal{I}_H\hat{u}_k^{\text{ms}}|_A + \|f\|_{L^2} + |g|_A\big)|v_H|_A. \end{aligned}$$

Inf-sup stability for a and $\tilde{a}$ finally gives, for any $v_H \in V_H$,

$$\begin{aligned} |\tilde{u}_k^{\text{ms}} - \hat{u}_k^{\text{ms}}|_A &\leq \tilde{\gamma}_0^{-1}\frac{|a(\tilde{u}_k^{\text{ms}} - \hat{u}_k^{\text{ms}}, v_H)|}{|v_H|_A} \\ &\lesssim \tilde{\gamma}_0^{-1}k^{d/2}\max(e_u, e_f, e_g)\big(|\mathcal{I}_H\hat{u}_k^{\text{ms}}|_A + \|f\|_{L^2} + |g|_A\big) \\ &\lesssim \tilde{\gamma}_0^{-1}\hat{\gamma}_0^{-1}k^{d/2}\max(e_u, e_f, e_g)\big(\|f\|_{L^2} + |g|_A\big). \end{aligned} \tag{23}$$

We conclude this section by presenting the main theoretical result of this paper. It gives a bound of the full error of $\hat{u}_k$ (in energy norm) in terms of the patch size k and the error indicators e_u, e_f, and e_g defined in Lemma 2. This theorem forms the basis for the implementation of a method that updates the multiscale space adaptively while iterating through the sequence of coefficients.

Theorem 4 (Error bound for multiscale method with lagging coefficient)**.** *Assume k is sufficiently large, so that $\gamma_k \geq \gamma_0$ holds. Let* $\mathrm{TOL} = ck^{-d/2}$ *and (by recomputation of element correctors)* $\max(e_u, e_g, e_f) \leq \mathrm{TOL}$*. Choose c sufficiently small so that $\tilde{\gamma}_k \geq \tilde{\gamma}_0$, and $\hat{\gamma}_k \geq \hat{\gamma}_0$. Further, let u solve* (3) *and $\hat{u}_k^{\mathrm{ms}}$ solve* (13)*. Let $\hat{u}_k = \hat{u}_k^{\mathrm{ms}} + \tilde{\mathcal{R}}_k f - \tilde{\mathcal{Q}}_k g$. Then*

$$|u - \hat{u}_k|_A \lesssim k^{d/2}(\theta^k + \mathrm{TOL})(\|f\|_{L^2} + |g|_A),$$

where the hidden constant depends on the contrast but is independent of mesh size H, patch size k and regularity of the solution u.

Proof. The estimate of the full error $|u - \hat{u}_k|_A$ is obtained by combining (19), (21), and (23), and using the triangle inequality,

$$\begin{aligned}
|u - \hat{u}_k|_A &\leq |u - u_k|_A + |u_k - \tilde{u}_k|_A + |\tilde{u}_k - \hat{u}_k|_A \\
&\lesssim k^{d/2}\Big((1 + \gamma_0^{-1})\theta^k + ((1 + \tilde{\gamma}_0^{-1})\gamma_0^{-1} + \tilde{\gamma}_0^{-1}\hat{\gamma}_0^{-1})\max(e_u, e_f, e_g)\Big)\cdot \\
&\quad \cdot (\|f\|_{L^2} + |g|_A) \\
&\lesssim k^{d/2}(\theta^k + \max(e_u, e_f, e_g))(\|f\|_{L^2} + |g|_A)
\end{aligned}$$

and finally using the assumed bounds of e_u, e_f and e_g. □

5 Implementation

In this section, we present two algorithms for computing approximate solutions to a sequence of problems as described by (1). In a practical implementation we can not let V be an infinite dimensional space. We will assume that there is a finite element space V_h based on a mesh that resolves the coefficient, which if used to solve (3), yields an approximate solution u_h with satisfactory small error $|u - u_h|_A$. The analysis in the previous sections holds also if replacing V with V_h, however, the error estimates will then of course be bounding $|u_h - \hat{u}_k|_A$ instead of $|u - \hat{u}_k|_A$. We study the memory requirements for both algorithm. The second algorithm is constructed to minimize the memory requirements.

5.1 Full algorithm

In this section we present an algorithm that computes the full fine-scale solution. The key idea is that, as time n progresses, we do not update the full multiscale space, but only the parts where it is necessary for a sufficiently small error. If A^n only changes slightly between two consecutive n, it is

possible that many of the element correctors ($\tilde{\mathcal{Q}}_{k,T}v_H$, $\tilde{\mathcal{R}}_{k,T}f$ and $\tilde{\mathcal{Q}}_{k,T}g$) based on lagging coefficients do not need to be recomputed. We use the error indicators e_u, e_f and e_g to determine for which elements to recompute correctors. This results in an algorithm that is completely parallelizable over T, except for the solution of the low-dimensional (posed in V_H) global system. Even the assembly of the global stiffness matrix $\mathbf{K} = (K_{ij})_{ij}$ and right hand side $\mathbf{b} = (b_i)_i$ can be done in parallel, as it becomes a reduction over T.

The algorithm is presented in Algorithm 1. We denote by $\phi_i \in V_H$, $i = 1, 2, \ldots$ the finite element basis functions spanning V_H.

Algorithm 1: Full algorithm

```
Pick k, TOL and number of time steps N
Let Ã_T ← A^1 for all T
Compute Q̃_{k,T}φ_i, R̃_{k,T}f and Q̃_{k,T}g for all T and i          eq. (9)
for n = 1, ..., N do
    Let A ← A^n be the true coefficient for this time step
    for all T do
        Compute e_{u,T}, e_{f,T} and e_{g,T}                        Lemma 2
        if max(e_{u,T}, e_{f,T}, e_{g,T}) ≥ TOL then
            Update lagging coefficient Ã_T ← A^n
            Recompute Q̃_{k,T}φ_i, R̃_{k,T}f and Q̃_{k,T}g             eq. (9)
        Update K_ij += ã_T(φ_j, φ_i) using Q̃_{k,T}φ_i               eq. (11)
        Update b_i += L̃_T(φ_i) using R̃_{k,T}f and Q̃_{k,T}g          eq. (12)
    Solve for û_k^ms, by computing K^{-1}b                          eq. (13)
    Compute û_k = û_k^ms + R̃_k f − Q̃_k g if needed
```

Note that the **if**-statement in this algorithm together with properly chosen k and TOL, ensure that the conditions for Theorem 4 are fulfilled. The numerical experiment in Section 6.1 investigates the relations between the error and TOL and the fraction of recomputed element correctors.

5.1.1 Memory consumption

The memory required to perform the full algorithm grows with k in the following manner. Suppose $\mathcal{O}(h^{-d})$ is the number of elements in the fine discretizations, as is the case for quasi-uniform meshes. To compute e_u, e_f and e_g, we need to keep $\tilde{A}_T$, $\tilde{\mathcal{Q}}_{k,T}\phi_i$, $\tilde{\mathcal{R}}_{k,T}f$, and $\tilde{\mathcal{Q}}_{k,T}g$ between the iterations in Algorithm 1 (see Lemma 2). Since the patches $U_k(T)$ overlap by $\mathcal{O}(k^d)$ coarse elements, the amount of memory required between the iterations scales like $\mathcal{O}(k^d h^{-d})$. In high dimensions for very fine meshes, the amount of memory needed for storage can become a limitation. Next, we study an application

where it is possible to reduce the memory requirements.

5.2 Upscaling algorithm

In this section we illustrate a case in the context of two-phase Darcy flow where it is possible to reduce the space complexity to $\mathcal{O}(k^d H^{-d})$. This is done by solving the hyperbolic transport equation on the coarse mesh and the pressure equation with saturation dependent diffusion coefficient on a fine mesh using the proposed adaptive multiscale method. This is a typical situation, since homogenization of the diffusion coefficient in the pressure equation is not possible by averaging. The low space complexity and the possibility to parallelize the corrector computations enable large-scale computations.

5.2.1 Discretization of two-phase Darcy flow problem

Consider the two-phase Darcy flow equations in (2). The permeability K varies on a fine scale, requring these variations to be resolved by a fine mesh with mesh size h. We assume, however, that the saturation equation needs only be solved on a coarse mesh with mesh size $H > h$ to obtain a sufficiently accurate solution. Thus, in addition to the coarse mesh $\mathcal{T}_H$, we introduce a fine mesh $\mathcal{T}_h$ which is a refinement of the former. The pressure and saturation equations are solved sequentially: Given initial data for the saturation, the pressure equation is solved. An approximation of the coarse element face flux is computed and used to solve for the next saturation using a zeroth order upwind discontinuous Galerkin method with explicit Euler forward time-stepping.

We use the same discretization scheme as in [17]. Let $P_0(\mathcal{T}_H)$ be the space of piecewise constants on the elements of $\mathcal{T}_H$. Let $\mathcal{F}_H$ denote set of faces of $\mathcal{T}_H$. Each face $F \in \mathcal{F}_H$ has a normal direction $\mathbf{n}_F$ (outward pointing for boundary faces). We define the jump operator over face F as $[\![v]\!] = (v|_{T_1})|_F \mathbf{n}_1 \cdot \mathbf{n}_F + (v|_{T_2})|_F \mathbf{n}_2 \cdot \mathbf{n}_F$, where $\mathbf{n}_1$ and $\mathbf{n}_2$ are the outward pointing face normals of the two elements T_1 and T_2 adjacent to F. Let $\langle \cdot, \cdot \rangle_\omega$ denote the L^2-scalar product when ω is $d-1$-dimensional. We let the flow be completely driven by boundary conditions, i.e. $f = 0$. We use the following discretization for the saturation equation. Given $s_H^{n-1} \in P_0(\mathcal{T}_H)$, $\sigma^n \in L^1(\mathcal{F}_H)$, find $s_H^n \in P_0(\mathcal{T}_H)$ such that for all $r_H \in P_0(\mathcal{T}_H)$,

$$\begin{aligned} \Delta t^{-1}(s_H^n - s_H^{n-1}, r_H) = &-\langle \psi(s_{H,\text{upw}}^{n-1})\sigma^n, [\![r_H]\!] \rangle_{\mathcal{F}_{H,I}} - \\ &\langle \psi(s_H^{n-1})\sigma^n, r_H \rangle_{\mathcal{F}_{H,\text{out}}} - \langle \psi(s_B)\sigma^n, r_H \rangle_{\mathcal{F}_{H,\text{in}}}. \end{aligned} \tag{24}$$

Here σ^n is an upscaled total flux quantity approximating (over face F) $\sigma^n|_F \approx -\mathbf{n}_F \cdot \lambda(s) K \nabla(u+g)$; the sets $\mathcal{F}_{H,I}$, $\mathcal{F}_{H,\text{out}}$, and $\mathcal{F}_{H,\text{in}}$ contain interior faces,

Dirichlet boundary faces with outgoing and ingoing flux, respectively; s_B is the saturation boundary condition; and $s^n_{H,\text{upw}}$ is the upwind saturation

$$s^n_{H,\text{upw}}|_F = \begin{cases} (s^n_H|_{T_1})|_F, & \text{if } \sigma^n \geq 0, \\ (s^n_H|_{T_2})|_F, & \text{if } \sigma^n < 0, \end{cases} \tag{25}$$

where T_1 and T_2 are adjacent to F and $\mathbf{n}_F$ points from T_1 to T_2; and the function $\psi(s) = \lambda_w(s)/\lambda(s)$ is the so called fractional flow function. The discretization of the pressure equation is: find $u^n_h \in V_h$, so that for all $v_h \in V_h$,

$$(A^n \nabla u^n_h, \nabla v_h) = -(A^n \nabla g, \nabla v_h), \tag{26}$$

where $A^n = \lambda(s^{n-1}_H)K$. As suggested in [17], we define the non-conservative pre-flux $\bar{\sigma}^n$ be a harmonic average of the (discontinuous) element face flux $-\mathbf{n}_F \cdot A^n \nabla(u_h + g)$ at the faces. Then we use the post-processing technique presented in [17] (with non-weighted minimization) to post-process $\bar{\sigma}^n$ and obtain the conservative flux σ^n used in the saturation equation.

We make two observations on the information exchange between the two equations when using this discretization:

1. In the pressure equation, we are only interested in the coarse scale saturation s^{n-1}_H from the saturation equation.

2. In the saturation equation, we are only interested in the upscaled flux $\int_F \sigma^n$ from the pressure equation.

5.2.2 Coarse error indicators

The first observation allows us to compute E_u, E_f and E_g from Section 3.5.1, without saving $\tilde{A}_T$. Suppose that for element T, the lagging coefficient $\tilde{A}_T = A^m$ is from time step $m < n$, and $A = A^n$. We note that δ_T is a coarse quantity, since fine-scale K cancels,

$$\delta_T = (\tilde{A}_T - A)A^{-1/2}\tilde{A}_T^{-1/2} = \frac{\lambda(s^{m-1}_H) - \lambda(s^{n-1}_H)}{\sqrt{\lambda(s^{m-1}_H)\lambda(s^{n-1}_H)}}. \tag{27}$$

Thus, to compute δ_T in (14), only $\tilde{\lambda}_{T,T'} := \lambda(s^{m-1}_H)|_{T'}$ for $T' \subset U_k(T)$ need to be saved from previous time steps. The space complexity of $\tilde{\lambda}_{T,T'}$ is $\mathcal{O}(k^d H^{-d})$. Also, $\tilde{\lambda}_{T,T'}$ can be used to compute $A^{-1/2}\tilde{A}_T^{1/2}$ in (14).

To summarize, no lagging fine scale information needs to be stored. Only the coarse quantities $\tilde{\mu}_{T,T'}$ and $\tilde{\lambda}_{T,T'}$ need to be saved between iterations.

5.2.3 Coarse face flux

The second observation is that we only need the coarse element face flux $\int_F \sigma^n$ for the saturation equation. Since this quantity is defined on the coarse mesh, we precompute

$$\begin{aligned}\tilde{\sigma}^n_{u,T,T',F,i} &= -\int_F \mathbf{n}_F \cdot \{\!\{\tilde{A}_T\}\!\}(\chi_T \nabla\phi_i - \nabla\tilde{\mathcal{Q}}_{k,T}\phi_i)|_{T'},\\ \tilde{\sigma}^n_{fg,T,T',F} &= -\int_F \mathbf{n}_F \cdot \{\!\{\tilde{A}_T\}\!\}\nabla(-\tilde{\mathcal{Q}}_{k,T}g + \tilde{\mathcal{R}}_{k,T}f)|_{T'},\end{aligned} \tag{28}$$

for all $T, T' \in \mathcal{T}_H$, for all faces $F \subset \overline{T'}$ and all basis functions ϕ_i with support in T. Here, we used the harmonic average $\{\!\{v\}\!\}|_F = 2\frac{(v|_{T_1})|_F (v|_{T_2})|_F}{(v|_{T_1})|_F + (v|_{T_2})|_F}$, where T_1 and T_2 are the two elements adjacent to F, if F is an interior face, and $\{\!\{v\}\!\}|_F = 2(v|_T)|_F$, where T is adjacent to F, if F is a boundary face. The memory required for storing $\tilde{\sigma}^n_{u,T,T',F,i}$ and $\tilde{\sigma}^n_{fg,T,T',F}$ scales with $\mathcal{O}(k^d H^{-d})$, since the two quantities are zero for all pairs (T', T) except when $T' \subset U_k(T)$.

If we now let the coarse component of the multiscale solution be expressed as $\mathcal{I}_H \hat{u}_k = \sum_i \alpha_i \phi_i$, then we can compute the upscaled non-conservative face flux by

$$\bar{\sigma}^n|_F = \frac{1}{2}\sum_{T,T',i} \alpha_i \tilde{\sigma}^n_{u,T,T',F,i} + \frac{1}{2}\sum_{T,T'} \tilde{\sigma}^n_{fg,T,T',F}.$$

The final conservative face flux $\sigma^n|_F$ is then computed using the post-processing technique developed in [17].

We conclude this section by listing the upscaling algorithm (Algorithm 2) for this two-phase Darcy flow problem. In this algorithm, the memory requirements are $\mathcal{O}(k^d H^{-d})$ (plus h^{-1} for coefficient A) which allows for very refined fine meshes. Also, the coarse element loop is still completely parallel, and this algorithm serves as a good candidate for a scalable memory efficient

upscaling algorithm.

Algorithm 2: Upscaling algorithm

Pick k, TOL and number of time steps N
Let $\tilde{A}_T \leftarrow \lambda(s_H^0)K$ for all T
Compute $\tilde{\mathcal{Q}}_{k,T}\phi_i$, $\tilde{\mathcal{R}}_{k,T}f$ and $\tilde{\mathcal{Q}}_{k,T}g$ for all T and i eq. (9)
Save only coarse quantities, $\tilde{\lambda}_{T,T'}$, $\tilde{\mu}_{T,T'}$, $\tilde{\sigma}^n_{u,T,T',F,i}$, and $\tilde{\sigma}^n_{fg,T,T',F}$
for $n = 1, \ldots, N$ **do**
  Let $A \leftarrow \lambda(s_H^{n-1})K$ be the true coefficient for this time step
  for *all* T **do**
    Compute $E_{u,T}$, $E_{f,T}$ and $E_{g,T}$ (using $\tilde{\lambda}_{T,T'}$, and $\tilde{\mu}_{T,T'}$) eq. (14)
    if $\max(E_{u,T}, E_{f,T}, E_{g,T}) \geq$ TOL **then**
      Update lagging coefficient $\tilde{A}_T \leftarrow \lambda(s_H^{n-1})K$
      Recompute $\tilde{\mathcal{Q}}_{k,T}\phi_i$, $\tilde{\mathcal{R}}_{k,T}f$ and $\tilde{\mathcal{Q}}_{k,T}g$
      Save only, $\tilde{\lambda}_{T,T'}$, $\tilde{\mu}_{T,T'}$, $\tilde{\sigma}^n_{u,T,T',F,i}$, and $\tilde{\sigma}^n_{fg,T,T',F}$
    Update K_{ij} += $\tilde{a}_T(\phi_j, \phi_i)$ using $\tilde{\mathcal{Q}}_{k,T}\phi_i$ eq. (11)
    Update b_i += $\tilde{L}_T(\phi_i)$ using $\tilde{\mathcal{R}}_{k,T}f$ and $\tilde{\mathcal{Q}}_{k,T}g$ eq. (12)
  Solve for $\hat{u}_k^{\text{ms}}$, by computing $\mathbf{K}^{-1}\mathbf{b}$ eq. (13)
  Compute resulting flux $\sigma^n|_F$ and solve for s_H^n eq. (24)

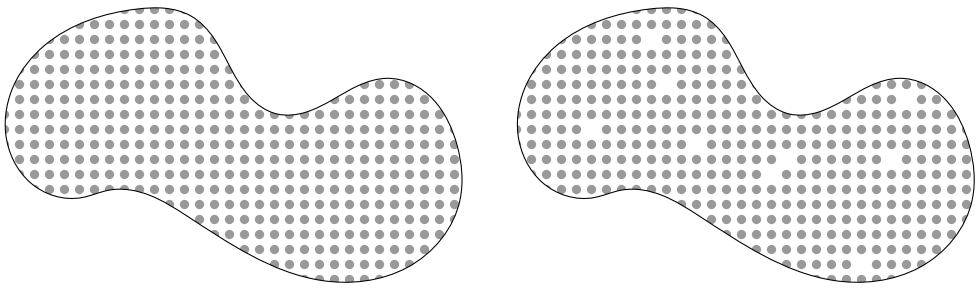

Figure 2: Defects in composite materials. Gray and white areas symbolizes two different values of the coefficient. Left: Reference material, lagging coefficient $\tilde{A}_T$. Right: Defect material, true coefficient A.

Remark 5 (Defects in composite materials)**.** *Although this paper has focused on time-dependent coefficients, we want to remark that the presented methods are also applicable to other applications. One such application is that of stochastic simulations on weakly random materials [1]. Consider the coefficient of a periodic reference material and a defect periodic material shown in Figure 2. If each ball in this material has a certain low probability to be*

missing (a point defect), the proposed method can be used to solve the problem with the defect material on the right (true coefficient) using correctors precomputed on the reference material on the left (lagging coefficient). In sample based methods for stochastic integration method (e.g. Monte Carlo), this method for determining what correctors to recompute can reduce the computational cost for the full simulation.

6 Numerical experiments

In all numerical experiments, we use $\mathcal{Q}_1$ Lagrange finite elements in 2D or 3D on rectangular or rectangular cuboid elements. The degrees of freedom are the values of the polynomial in the corners of the element.

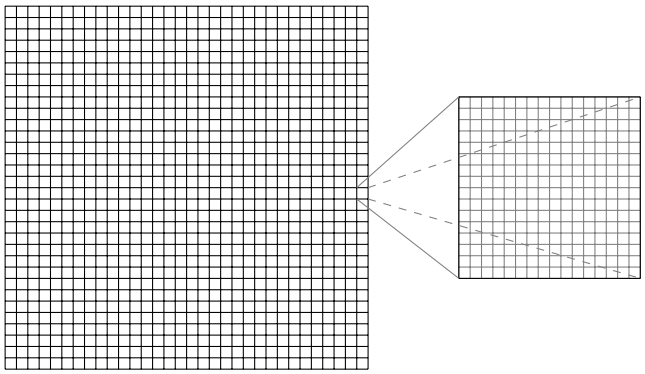

Figure 3: Illustrates a 32×32 coarse grid in 2D for V_H. To the right: A magnification of one coarse element revealing the fine discretization of V.

We define the interpolation operator $\mathcal{I}_H$ to be used throughout the experiments. Let P_1 denote the polynomials of no partial degree greater than 1, i.e. $\partial^2 p/\partial x^2 = 0$ for all independent variables x if $p \in P_1$. We define the broken finite element space,

$$S_{H,\mathrm{b}} = \{v \in L^2(\Omega) \,:\, v|_T \in P_1 \text{ for all } T \in \mathcal{T}_H\}.$$

We denote by Π_H the L^2-projection onto $S_{H,\mathrm{b}}$ and by $E_H : S_{H,\mathrm{b}} \to V_H$ the boundary condition conforming node averaging operator (Oswald interpolation operator), for all nodes in $\mathcal{T}_H$,

$$(E_H v)(x) = \begin{cases} 0 & \text{if } x \in \Gamma_D, \\ \mathrm{card}(T_x)^{-1} \sum_{T \in T_x} v|_T(x) & \text{otherwise,} \end{cases}$$

where $T_x = \{T \in \mathcal{T}_H \,:\, x \in \overline{T}\}$ and card is the cardinality. Then we define $\mathcal{I}_H = E_H \circ \Pi_H$. This operator satisfies (4), see e.g. [6].

6.1 Full algorithm experiment

We let $\Omega = [0,1]^2$, $\Gamma_D = \{x \in \partial\Omega : x_1 = 0 \text{ or } x_1 = 1\}$, $\Gamma_N = \partial\Omega \setminus \Gamma_D$, $f = 0$, $g = 1 - x_1$, and A_b as shown in Figure 4a. A was constructed by taking a uniform grid with 512×512 cells, and assigning each grid cell a value 10^c, where c was drawn from a uniform distribution between $[-2, 0]$, for each cell independently. Then, the values in cells whose midpoint $x_\mathrm{m} = (x_{\mathrm{m},1}, x_{\mathrm{m},2})$ satisfied $15/32 \leq x_{\mathrm{m},1} \leq 1/2$ were set to 10^{-2}. Finally, the values in cells whose midpoint x_m satisfied $1/4 \leq x_{\mathrm{m},2} \leq 5/16$ were set to 1. The space V is

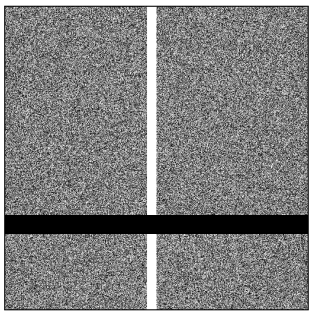

(a) Coefficient A_b. White means $A_\mathrm{b} = 10^{-2}$, black means $A_\mathrm{b} = 1$. The intensity of the grayscale scales linearly with $\log_{10}(A_\mathrm{b})$.

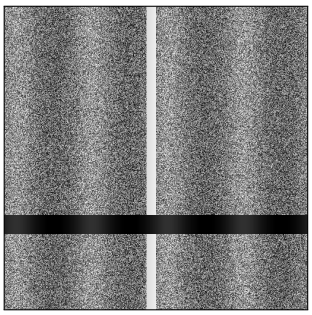

(b) Coefficient A_n for $n = 13$. The color scale spans $[10^{-2}, 3]$.

Figure 4: Coefficients for the full algorithm experiment.

discretized on a $\mathcal{Q}_1$ finite element space on a uniform grid of size 512×512, see Figure 3. The V_H is chosen as a $\mathcal{Q}_1$ finite element space on the coarse mesh shown in the same figure.

6.1.1 Error decay with k

First, we let $A = A_\mathrm{b}$ and solve for u_k for $k = 1, 2, 3$, and 4. We solve for u on the fine mesh and use that as reference solution. The exponential convergence in terms of k can be observed in Figure 5.

6.1.2 Sweeping change in coefficient

Now we fix $k = 3$ and define a sequence of coefficients A^n for $n = 0, \ldots, 127$,

$$A^n(x) = A_\mathrm{b}(x) \cdot (2 + \sin(8\pi(x_1 - n/128)))$$

This describes a perturbation of a factor up to 3 over the full domain, sweeping from the left to the right. We emphasize that the difference $A_{n+1} - A_n$ is

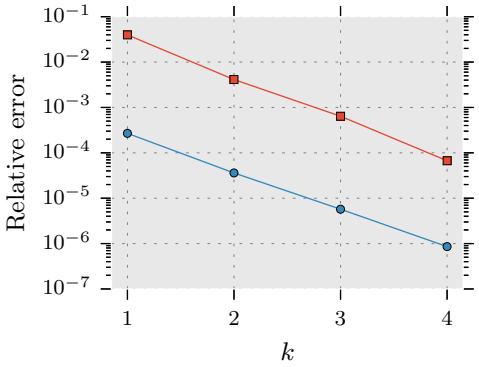

Figure 5: The data sets □ and ∘ correspond to the (relative) errors $|u - u_k|_A$ and $\|\mathcal{I}_H(u - u_k)\|_{L^2}$, respectively.

nonzero everywhere, which means a strategy to determine which correctors to recompute is necessary. We use Algorithm 1 to compute the approximate solution $\hat{u}_k$ for every time step n. A reference solution u is also computed. We do this for four values of TOL $= 0.5, 0.1, 0.05$, and 0.01.

The (relative) error in energy norm versus the time step n is plotted to the left in Figure 6. The right plot in the same figure shows the fraction of all element correctors $\tilde{\mathcal{Q}}_{k,T}$ that were recomputed in each time step. We note that the error decreases with decreasing TOL as expected and that the fraction of recomputed element correctors increase with decreasing TOL. Without an adaptive strategy, all element correctors would have to be recomputed in every time step. See Figure 7 for two maps over the recomputed element correctors in time step $n = 31$ for two different values of TOL.

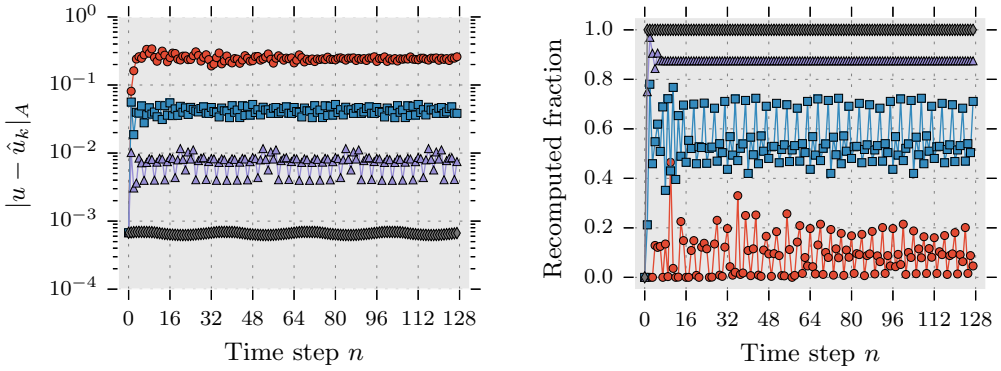

Figure 6: Error and recomputed fraction plots. The data sets ∘, □, △, and ◇ correspond to TOL $= 0.5, 0.1, 0.05$, and 0.01, respectively.

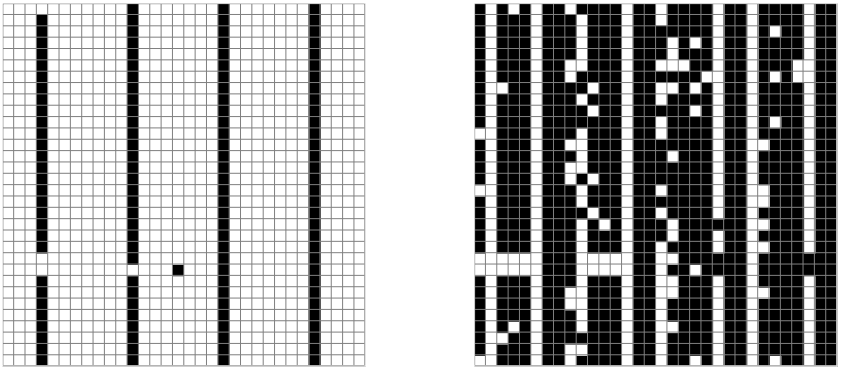

Figure 7: Time step $n = 31$. Elements T for which $\tilde{\mathcal{Q}}_{k,T}$ were recomputed are colored black. Left and right figure show the recomputed element correctors for TOL $= 0.5$ and TOL $= 0.1$, respectively.

6.2 Upscaling algorithm experiments

In the following two experiments, we investigate the properties of the upscaling algorithm presented in Section 5.2. We pick the following mobility functions $\lambda_w(s) = s^3$, $\lambda_n(s) = (1-s)^3$, and $\lambda(s) = \lambda_w(s) + \lambda_n(s)$.

6.2.1 2D random field data

We let $\Omega = [0,1]^2$, $\Gamma_D = \{x \in \partial\Omega : x_1 = 0 \text{ or } x_1 = 1\}$, $\Gamma_N = \partial\Omega \setminus \Gamma_D$, $f = 0$, $g = 1 - x_1$. We use a 512×512 rectangular grid as fine mesh for V_h and a 64×64 grid as coarse mesh for V_H. The permeability K is realized as a piecewise constant function on the fine mesh from a lognormal distribution with exponential spatial correlation and standard deviation 3, i.e. for a fine element midpoint x_{m},

$$K(x_{\mathrm{m}}) = \exp(3\kappa(x_{\mathrm{m}}))$$

where $\kappa(x_{\mathrm{m}}) \sim \mathcal{N}(0,1)$ and covariance between points are

$$\operatorname{cov}(\kappa(x), \kappa(y)) = \exp\left(\frac{-\|x-y\|_2}{d}\right),$$

with correlation length $d = 0.05$ and where $\|\cdot\|_2$ denotes Euclidian norm. The initial saturation is set to $s^0 = 0$, and boundary conditions are set to $s_B = 1$ on the left boundary, which is the only boundary with ingoing flux. The number of time steps and their size are set to $N = 2000$ and $\Delta t = N^{-1}$, respectively.

The upscaling algorithm was run with this setup with $k = 1, 2, 3$ and TOL $= 0.4$, 0.2, 0.1, 0.05, 0.025, and 0.0125. A reference solution $s^n_{H,\mathrm{ref}}$,

where the pressure equation was solved on the fine mesh using the Q_1 standard finite element method in every iteration was computed. To illustrate the need for upscaling, we also computed the pressure equation on the coarse mesh using the standard $\mathcal{P}_1$ finite elements. See Figure 8 for plots over the error in the saturaton solution at the final time step and average fraction of recomputed correctors. In the error plot we can see that both parameters k and TOL affect the error in the chosen regimes. We note from the recomputation plot that there is no dependency between the fraction of recomputed element correctors and patch size k. Figure 9 shows an example of the saturation solution and the number of times correctors have been computed.

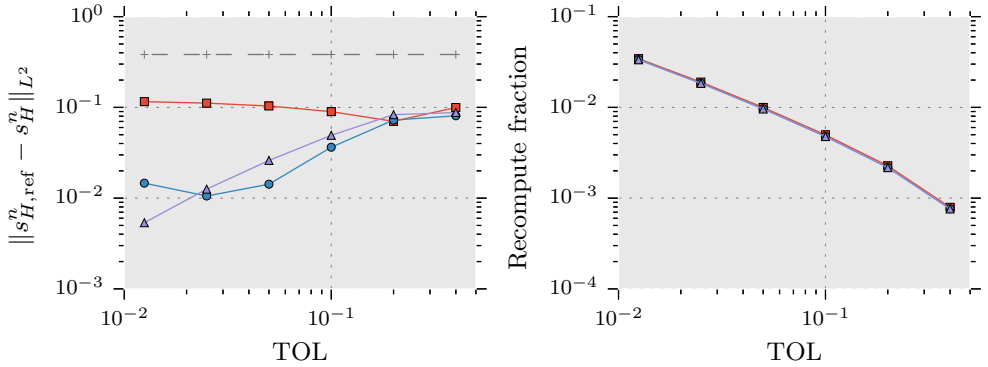

Figure 8: Error and recomputed fraction plots vs TOL. The data sets $\circ$, $\square$, and $\triangle$ correspond to $k = 1, 2$, and 3, respectively. The dashed line (+) is the error obtained if using the standard finite element method on the coarse mesh.

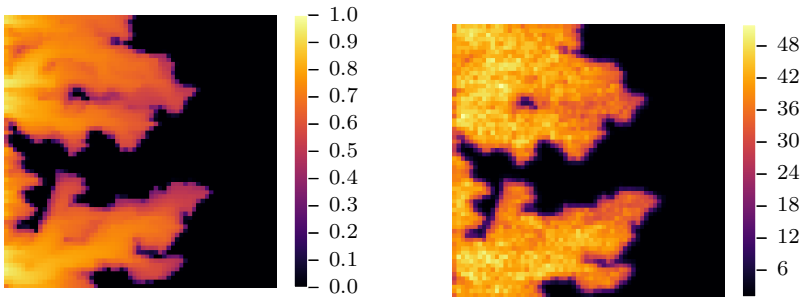

Figure 9: Time step $n = 2000$ for configuration $k = 2$ and TOL $= 0.05$. Left: Solution s^n_H. Right: Recompuation count for each element.

6.2.2 3D random field data

We let $\Omega = [0,1]^3$, $\Gamma_D = \{x \in \partial\Omega : x_1 = 0 \text{ or } x_1 = 1\}$, $\Gamma_N = \partial\Omega \setminus \Gamma_D$, $f = 0$, $g = 1 - x_1$. We use a $128 \times 128 \times 128$ rectangular grid as fine mesh for V_h and a $16 \times 16 \times 16$ grid as coarse mesh for V_H. We use a sample $\omega_{i,j,k,\ell}$ of independent uniformly distributed random numbers between 0 and 1. The permeability K is a piecewise constant function on the fine uniform mesh and is defined by

$$K(x_{\mathrm{m}}) = \frac{1}{2^{21}} \prod_{i=1}^{7} (1 + \omega_{i,\lceil 2^i x_{\mathrm{m},1} \rceil, \lceil 2^i x_{\mathrm{m},2} \rceil, \lceil 2^i x_{\mathrm{m},3} \rceil})^3,$$

where $x_{\mathrm{m}} = (x_{\mathrm{m},1}, x_{\mathrm{m},2}, x_{\mathrm{m},3})$ are the fine element midpoints, and $\lceil \cdot \rceil$ denotes the ceiling function. See Figure 10 for the particular realization used. The boundary conditions are set to $s_B = 0$ on the boundary with ingoing flux, and the initial saturation is set to a piecewise constant function s_H^0 on the coarse mesh with the following values in the coarse element midpoints x_{m},

$$s_H^0(x_{\mathrm{m}}) = \begin{cases} 1, & \text{if } \|x - \frac{1}{2}(1,1,1)\|_2 \leq \frac{1}{4}, \\ 0, & \text{otherwise.} \end{cases}$$

The number of time steps are set to $N = 200$ and the time step to $\Delta t = 1$.

The upscaling algorithm was run for the three parameter combinations I: $k = 1$, TOL $= 0.1$, II: $k = 2$, TOL $= 0.1$, and III: $k = 1$, TOL $= 0.01$. Figure 10 gives an illustration of the solution at $n = 0$ and $n = 200$. One of the images shows the recomputed elements as blue boxes and we can see that many elements are not recomputed. In this case, we were not able to compute a reference solution using the available computational resources. But we can estimate the sensitivity of the solutions with respect to the parameters k and TOL. Let $s_{H,\mathrm{I}}^{200}$, $s_{H,\mathrm{II}}^{200}$, and $s_{H,\mathrm{III}}^{200}$ denote the saturation solutions at time step $n = 200$ for the parameter combinations I, II, and III, respectively. We get

$$\begin{aligned} \text{vary } k: &\quad \|s_{H,\mathrm{I}}^{200} - s_{H,\mathrm{II}}^{200}\|_{L^2(\Omega)} = 0.0065, \quad \|s_{H,\mathrm{I}}^{200} - s_{H,\mathrm{II}}^{200}\|_{L^\infty(\Omega)} = 0.0664, \\ \text{vary TOL}: &\quad \|s_{H,\mathrm{I}}^{200} - s_{H,\mathrm{III}}^{200}\|_{L^2(\Omega)} = 0.0019, \quad \|s_{H,\mathrm{I}}^{200} - s_{H,\mathrm{III}}^{200}\|_{L^\infty(\Omega)} = 0.0242. \end{aligned}$$

These numbers suggest that the parameter k, i.e. error due to localization dominates in this case.

7 Conclusion

Elliptic equations with similar rapidly varying coefficients occur for instance in time-dependent problems for two-phase Darcy flow and in stochastic simulations on defect composite materials. We consider a sequence of elliptic

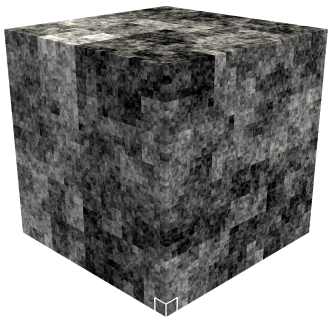

(a) Coefficient on fine mesh. The coarse element size can be seen in the closest corner.

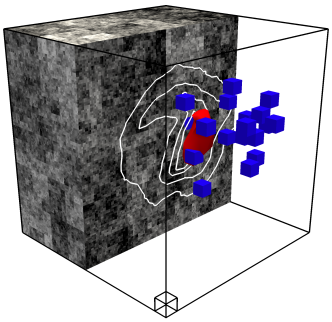

(b) Time step $n = 200$. Blue elements have been recomputed this time step.

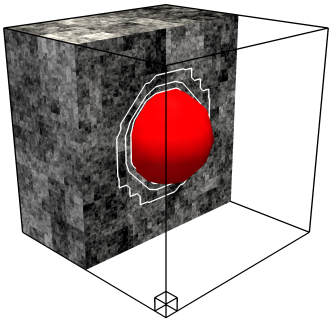

(c) A slice of the initial conditions at time step $n = 0$.

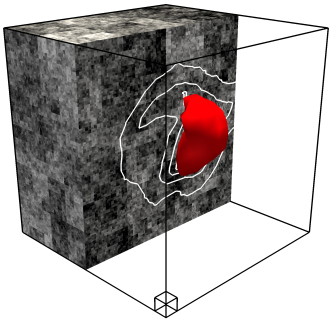

(d) A slice of the solution at time step $n = 200$.

Figure 10: The gray solid is the coefficient $1.42 \times 10^{-6} \leq K \leq 0.46$. The red shape is the isosurface for $s = 0.75$. The white lines are isolines for $s = 0.1$, 0.5, 0.75 and 0.9 at the slice, which is the plane $x_2 = 0.5$. The solutions and recomputed elements are shown for the case $k = 1$, TOL $= 0.1$

equations, each with different coefficients A^n, $n = 1, 2, \ldots$. We define a method that computes and updates an LOD multiscale space as we iterate through the coefficients. This is done by the computation of localized element correctors that depend on the coefficient in the vicinity of the element. We derive error indicators $e_{u,T}$, $e_{f,T}$, and $e_{g,T}$ that indicate whether or not to update the corrector at element T while iterating the sequence of coefficients. By selecting a small enough tolerance TOL for the error indicators, the multiscale space will keep its approximation properties through the sequence of coefficients. It is shown analytically and numerically that the error indicators bound the error in energy norm of the solution. We further present a memory efficient upscaling algorithm for a particular application of two-phase Darcy flows.

References

[1] A. Anantharaman and C. L. Bris. A numerical approach related to defect-type theories for some weakly random problems in homogenization. *Multiscale Model. Simul.*, 9(2):513–544, 2011.

[2] I. Babuška and J. E. Osborn. Generalized finite element methods: Their performance and their relation to mixed methods. *SIAM J. Numer. Anal.*, 20(3):510–536, 1983.

[3] M. Bebendorf. Low-rank approximation of elliptic boundary value problems with high-contrast coefficients. *SIAM J. Numer. Anal.*, 48(2):932–949, 2016.

[4] A. Bensoussan, J. L. Lion, and G. Papanicolaou. *Asymptotic Analysis for Periodic Structure*, volume 5 of *Studies in Mathematics and Its Applications*. North-Holland, Amsterdam, 1978.

[5] Z. Chen, G. Huan, and B. Li. An improved IMPES method for two-phase flow in porous media. *Transp. Porous Media*, 54(3):361–376, 2004.

[6] D. A. Di Pietro and A. Ern. *Mathematical Aspects of Discontinuous Galerkin Methods*. Springer-Verlag Berlin Heidelberg, 2012. Mathématiques et Applications, Vol. 69.

[7] D. Elfverson, V. Ginting, and P. Henning. On multiscale methods in Petrov–Galerkin formulation. *Numer. Math.*, 131(4):643–682, 2015.

[8] F. Hellman and A. Målqvist. Contrast independent localization of multiscale problems. *arXiv:1610.07398*, 2016.

[9] R. Helmig. *Multiphase flow and transport processes in the subsurface*. Springer-Verlag, Berlin Heidelberg, 1997.

[10] P. Henning and A. Målqvist. Localized orthogonal decomposition techniques for boundary value problems. *SIAM J. Sci. Comput.*, 36(4):A1609–A1634, 2014.

[11] T. Y. Hou and X.-H. Wu. A multiscale finite element method for elliptic problems in composite materials and porous media. *J. Comput. Phys.*, 134(1):169 – 189, 1997.

[12] T. J. R. Hughes, G. R. Feijóo, L. Mazzei, and J.-B. Quincy. The variational multiscale method—a paradigm for computational mechanics. *Comput. Methods Appl. Mech. Engrg.*, 166(1-2):3–24, 1998.

[13] T. J. R. Hughes and G. Sangalli. Variational multiscale analysis: the fine-scale green's function, projection, optimization, localization, and stabilized methods. *SIAM J. Numer. Anal.*, 45(2):539–557, 2007.

[14] R. Kornhuber and H. Yserentant. Numerical homogenization of elliptic multiscale problems by subspace decomposition. *Multiscale Model. Simul.*, 14(3):1017–1036, 2016.

[15] A. Målqvist and D. Peterseim. Localization of elliptic multiscale problems. *Math. Comp.*, 83(290):2583–2603, 2014.

[16] J. Nordbotten and M. A. Celia. *Geological Storage of CO_2: Modeling Approaches for Large-Scale Simulation*. John Wiley & Sons, Inc., Hoboken, New Jersey, 2012.

[17] L. H. Odsæter, M. F. Wheeler, T. Kvamsdal, and M. G. Larson. Post-processing of non-conservative flux for compatibility with transport in heterogeneous media. *Computer Methods in Applied Mechanics and Engineering*, 315:799 – 830, 2017.

[18] H. Owhadi, L. Zhang, and L. Berlyand. Polyharmonic homogenization, rough polyharmonic splines and sparse super-localization. *ESAIM Math. Model. Numer. Anal.*, 48(2):517–552, 2014.

[19] D. Peterseim and R. Scheichl. Robust numerical upscaling of elliptic multiscale problems at high contrast. *Comput. Meth. in Appl. Math.*, 16(4):579–603, 2016.